Carbon 136 (2018) 85–93

Contents lists available at ScienceDirect

Carbon

journal homepage: www.elsevier.com/locate/carbon

Perspectives

Measured *in-situ* mass absorption spectra for nine forms of highly-absorbing carbonaceous aerosol☆

Christopher D. Zangmeister [a, *, 1], Rian You [a, b, 1], Elizabeth M. Lunny [c, 1], Arne E. Jacobson [d], Mitchio Okumura [c], Michael R. Zachariah [a, b], James G. Radney [a, 1]

[a] Material Measurement Laboratory, National Institute of Standards and Technology, Gaithersburg, MD, 20899, USA
[b] Department of Chemistry and Biochemistry, University of Maryland College Park, College Park, MD, 20742, USA
[c] Division of Chemistry and Chemical Engineering, California Institute of Technology, Pasadena, CA, 91125, USA
[d] Environmental Resources Engineering, Humboldt State University, Arcata, CA, 95521, USA

ARTICLE INFO

Article history:
Received 8 December 2017
Received in revised form
19 April 2018
Accepted 21 April 2018
Available online 23 April 2018

ABSTRACT

Mass absorption coefficient spectra were measured between $\lambda = 500$ nm and 840 nm for nine forms of highly-absorbing carbonaceous aerosol: five samples generated from gas-, liquid- and solid-fueled flames; spark-discharge fullerene soot; graphene and reduced graphene oxide (rGO) crumpled nanosheets; and fullerene (C_{60}) assemblies. Aerosol absorption spectra were measured for size- and mass-selected particles and found to be dependent on fuel type and formative conditions. Flame-generated particles had morphologies consistent with freshly emitted black carbon (BC) with mass absorption coefficients *(MAC)* ranging between 3.8 $m^2\,g^{-1}$ and 8.6 $m^2\,g^{-1}$ at $\lambda = 550$ nm. Absorption Ångström exponents (*AAE*) – i.e. *MAC* spectral dependence – ranged between 1.0 and 1.3 for flame-generated particles and up to 7.5 for C_{60}. The dependence of *MAC* and *AAE* on mobility diameter and particle morphology was also investigated. Lastly, the current data were compared to all previously published *MAC* measurements of highly-absorbing carbonaceous aerosol.

Published by Elsevier Ltd.

1. Introduction

Highly-absorbing carbonaceous aerosol forms during the incomplete combustion of carbon-containing fuels. Due to the diversity of matter in the atmosphere, black carbon aerosol (BC) has been delineated from other suspended carbonaceous nanomaterials and narrowly defined by its chemical, physical and spectroscopic properties. BC is composed of nearly-elemental carbon with extended sp^2-bonding between carbon atoms arranged in multi-layered graphene-like sheets forming concentric, spherical nanoscale monomers aggregated into an open, lacey structure [1,2], see Fig. 1. The lacey aggregates may rearrange (collapse) into a compact, spherical, void-filled morphology after interaction with condensed- and/or gas-phase species [3–5]. Other similar carbonaceous nanomaterials can form under different conditions impacting the material's physical and, potentially, spectroscopic properties. For example, graphene and reduced graphene oxide (rGO) form crumpled nanopaper-like structures [6–9], see Fig. 1, chemically analogous to BC but morphologically dissimilar. It is unclear how, or if, these properties impact light absorption.

BC is spectroscopically defined as a material with a mass-specific (mass-normalized) absorption cross-section of 7.5 ± 1.2 $m^2\,g^{-1}$ at $\lambda = 550$ nm, the solar transmission maximum [1]. From the Beer-Lambert Law, the absorption coefficient (α_{abs}, m^{-1}) is the product of the number density of absorbers (N, m^{-3}) and their corresponding absorption cross-sections (C_{abs}, m^2)

$$\alpha_{abs} = N{*}C_{abs} = N{*}m_p{*}MAC = M{*}MAC \quad (1)$$

If particle mass (m_p, g), or the ensemble mass concentration (M, g m^{-3}) is known, it is possible to parameterize α_{abs} in terms of *MAC* ($m^2\,g^{-1}$). In the small particle (i.e. Rayleigh regime) or optically-thin limits where absorption scales directly with mass (volume) [10,11], *MAC* represents the mass-specific absorption cross-section. Otherwise, *MAC* represents the mass absorption coefficient; in some studies, the mass absorption efficiency (*MAE*) is also used [12–15]. In comparison to solution-phase spectroscopy, the mass-specific absorption cross-section and the mass absorption

☆ All authors have given approval of the final version of the manuscript.
* Corresponding author.
E-mail address: cdzang@nist.gov (C.D. Zangmeister).
[1] These authors contributed equally to this work.

https://doi.org/10.1016/j.carbon.2018.04.057
0008-6223/Published by Elsevier Ltd.

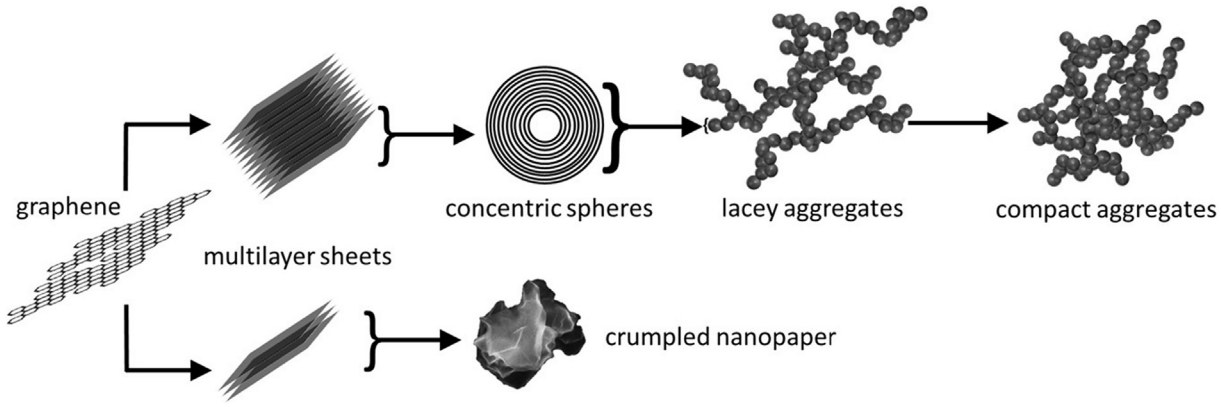

Fig. 1. Schematic of formation for graphene-based highly-absorbing carbonaceous nanomaterials. Top shows graphene-like sheets stacking and forming nanoscale concentric spheres that aggregate into lacey structures resembling freshly formed BC. Aggregates may become compacted upon interaction with gaseous or condensed phase materials. Bottom shows graphene-like material in single or multilayer sheets forming a nanoscale crumpled-paper morphology.

coefficient approximate the linear and non-linear regimes in absorption as a function of absorber number density (e.g. dilute and high concentration limits), respectively. For the remainder of this manuscript, *MAC* is used to refer to the mass absorption coefficient as the measured values of highly-absorbing carbonaceous particles may be size (mass) dependent (see Fig. 5a and corresponding discussion). The wavelength dependence of *MAC* can be described by the absorption Ångström exponent (*AAE*)

$$MAC_{\lambda} = MAC_{\lambda,0}\left(\frac{\lambda}{\lambda_0}\right)^{-AAE} \quad (2)$$

where λ and λ_0 are an arbitrary wavelength and a reference wavelength, respectively [16,17].

BC exhibits the second largest direct positive radiative forcing after CO_2 [1,18,19]. Quantitative assessment of an aerosol's radiative forcing requires its spectroscopic properties to be well-known with minimal uncertainty across the ultraviolet to near-IR. The most comprehensive assessments of highly-absorbing carbonaceous aerosols were reviews by Bond and Bergstrom (2006) [1] and Bond et al. (2013) [18] which focused on determination of BC *MAC* using data from peer-reviewed publications. The previously published data were corrected to account for presumed measurement biases and normalized to $\lambda = 550$ nm assuming an *AAE* of 1 (λ^{-1}); i.e. particles in the Rayleigh regime with a wavelength independent complex refractive index ($m = n + ik$) over the desired wavelength interval [10,11]. The studies used by Bond and Bergstrom (2006) [1] reported a BC *MAC* ranging from 1.6 $m^2\,g^{-1}$ to 15.9 $m^2\,g^{-1}$ with an average of 7.5 ± 1.2 $m^2\,g^{-1}$ (1σ) at $\lambda = 550$ nm. Notably, none of the studies used in the assessments directly measured *MAC* due to a lack, at the time, of reliable methods to measure aerosol mass *in-situ*. In addition to the determination of radiative forcing from BC, measured *in-situ* spectral properties, such as aerosol absorption and *AAE*, have also been used for aerosol identification and source apportionment [20,21].

The most direct method of obtaining *MAC* is to measure all experimental parameters: e.g. ensemble absorption coefficients and average particle mass and number density, ensemble absorption coefficients and mass concentration or single-particle absorption cross-section and mass. Aerosol metrology, such as mass selectivity and *in-situ* spectroscopies, has improved significantly since the 2006 BC *MAC* assessment enabling re-assessment. Newly developed techniques have highlighted the need for intercomparability of laboratory methods and the development of aerosolizable materials for standards [22,23]. This investigation explores particle absorption for size- and mass-selected highly-absorbing carbonaceous aerosol. The goal is to establish the range of mass-normalized aerosol absorption for this important class of atmospherically relevant materials under controlled conditions and compare these data to other studies. *MAC* of nine types of highly-absorbing carbonaceous aerosol was determined from measurements of α_{abs}, m_p and N using a photoacoustic spectrometer coupled to a broad-bandwidth ($\lambda = 500$ nm–840 nm) light source, an aerosol particle mass analyzer and a condensation particle counter, respectively. Particles were generated from multiple sources to understand how aerosol formation conditions and material properties impact absorption. These data were compared to over four decades of published absorption data to aid in bounding the range of *MAC* measurements for this family of carbonaceous particles.

2. Materials and methods

A general experimental schematic is shown in Fig. 2. Aerosol generation was specific for each sample and is described below. Aerosol was dried and mobility- and mass-classified using a differential mobility analyzer (DMA) and an aerosol particle mass analyzer (APM), respectively, prior to measurements of absorption coefficients and number density using a photoacoustic spectrometer (PA) and condensation particle counter (CPC), respectively.

2.1. Aerosol generation

Carbon black (0.25 mg mL^{-1}, Cab-*O*-Jet® 200, Cabot Corp., Lot # 3404296) [24], graphene nanoplatelets (4 mg mL^{-1}, Graphene Supermarket #A-12) and fullerene soot (4 mg mL^{-1}, Alfa-Aesar #40971) particles were generated from aqueous solution in a constant-output liquid-jet cross-flow atomizer (TSI 3076) supplied with dry air (dew point < −73 °C) at 30 psig. Of the 2.2 L min^{-1} of generated flow, 0.5 L min^{-1} was sampled for measurements while the remainder was exhausted in a laboratory snorkel. For generation of thermally reduced graphene oxide (rGO) [25], graphene oxide (GO, 4 mg mL^{-1}, ACS Material, LLC) was atomized from aqueous solution. After drying, the aerosol stream was passed through a tube furnace (Lindberg-Blue Mini-Mite) at 320 °C to thermally reduce the GO. Any additional water produced during reduction was removed via passage through a secondary drying stage. For generation of graphene nanoplatelets and fullerene soot particles, the supply bottle was immersed in an ultrasonicator during atomization to mechanically suspend material in solution.

Fullerene (C_{60}) particles were generated through vaporization

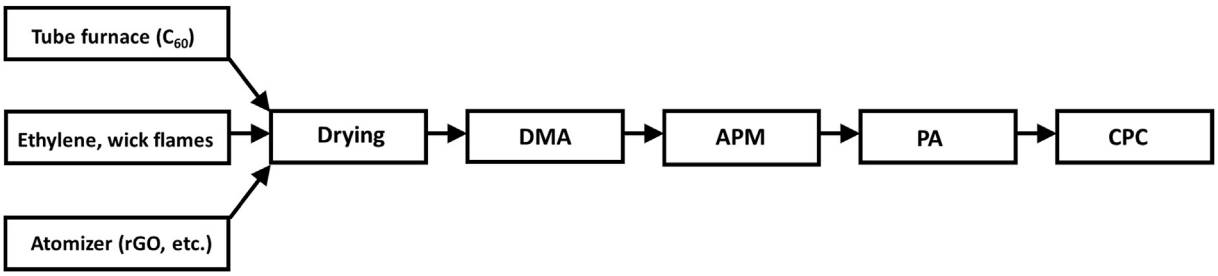

Fig. 2. Experimental schematic for absorption measurements. Drying was used for flame- and atomizer-generated particles. A differential mobility analyzer (DMA) and aerosol particle mass analyzer (APM) were used for particle mobility- and mass-classification, respectively. Absorption spectra were measured using a broadband photoacoustic spectrometer (PA). Particle number density was measured using a condensation particle counter (CPC).

and condensation of powdered C_{60} (SES Research #600-9969) in a tube furnace maintained at 650 °C in a flow of Ar at 1.5 L min^{-1} [26]. No drying elements were used. Of the supplied flow, 0.5 L min^{-1} was sampled for measurements with the remainder exhausted in a laboratory snorkel.

Particles from ethylene fuel were generated from a Santoro diffusion flame [27]. Particles were aspirated into 5 L min^{-1} of dry, HEPA-filtered air via a 1 mm diameter inlet on a sampling tube located 5 cm above burner centerline. An ejector pump located downstream mixed the particle stream with an additional 10 L min^{-1} of dry HEPA-filtered air. Of this flow, 0.5 L min^{-1} was sampled for measurements with the remainder exhausted in a fume hood.

Particles from kerosene and diesel fuel were generated from a simple wick lamp made in-house and modeled after typical sources used in developing countries [28,29]. The simple wick lamp was fueled with USA grade 1-K Kerosene (Klean Strip) or ultra-low sulfur diesel (NIST Emergency Services Facility fueling station, Gaithersburg, MD) using a 3.175 mm diameter braided cotton wick (Pepperell Braiding Company #1115-S) maintained at 1.0–1.5 mm above the lip of the lamp. The lamp was operated inside a 56 cm long, 8.25 cm I.D. glass shroud with >50 L min^{-1} of sheath flow. Under these conditions, the flame height was ≈1 cm. Particles were sampled through an inlet 2.54 cm in diameter directed downward towards the flame, located ≈7.5 cm above the wick terminus and drawing 0.5 L min^{-1} of flow. Excess flow was exhausted in a laboratory snorkel.

Particles from paraffin wax were generated from candles poured in-house using wax obtained from King of Heaven candles (Rok Ind. Ltd., Nairobi, Kenya) and a 3.175 mm diameter braided cotton wick (Pepperell Braiding Company #1115-S). Wicks were maintained at ≈ 1.25 cm during combustion and particles were sampled similarly to the liquid-fuel simple wick lamps.

2.2. Aerosol conditioning and classification

Water was removed prior to particle size- and mass-classification by passing the aerosol stream through a large-diameter Nafion drying tube (Perma Pure, LLC #MD-700-48F-1) with a 20:1 parallel flow of dry air (<5% relative humidity) and a pair of silica gel diffusion dryers (TSI #3062) prior to size (electrical mobility) selection by a DMA (TSI Long DMA #3081). The relative humidity inside the DMA was monitored to ensure it was stable (<10% relative humidity) for the duration of an experiment to avoid interferences from both gas and liquid water [16,30,31]. Sheath:aerosol flow in the DMA was maintained at 10:1 by the recirculating pumps in the electrostatic classifier (TSI #3082). After size selection, particles were passed through an APM (Kanomax #3602), a PA and a CPC (TSI #3775) in series. To ensure only particles bearing $q = +1$ were measured by the PA [32], we followed recommendations put forth in Radney and Zangmeister (2016) [33] for tandem DMA/APM measurements.

For C_{60} (generated in Ar), the DMA was operated in a single-pass mode. Dry, HEPA-filtered air was supplied from a compressed air line and removed via vacuum pump with the sheath:aerosol volumetric flow maintained at 10:1 using a pair of mass flow controllers (MKS #1179C). The resulting sample airstream exiting the DMA contained ≈10% Ar.

2.3. Photoacoustic spectroscopy

MAC spectra spanning $\lambda = 500$ nm–840 nm were measured using a PA equipped with a supercontinuum laser and tunable wavelength and bandpass filter, as in Radney and Zangmeister (2015) [16] and the Supporting Information of Radney et al. (2017) [34]. Absorption coefficients (α_{abs}), mass (m_p) and particle number densities (N) were calculated from 1 Hz data and averaged to 30 s; wavelength regions were alternated at 30 s intervals. In total, 3 spectra were collected and averaged to a single replicate. For each replicate, *MAC* at each wavelength was then calculated through the second form of Eq. (1) ($MAC = \alpha_{abs}/m_p N$). *MAC* values from a minimum of 3 replicates were averaged for all reported spectra; reported measurement uncertainties represent 2 times the standard deviation of all replicates at a given wavelength. From these measurements, material effective density (ρ_{eff}) was also determined ($\rho_{eff} = 6m_p/\pi D_m^3$) where D_m is the particle mobility diameter. Prior to measurement of C_{60} aerosol, the frequency response of the acoustic resonator was measured to determine the resonant frequency, resonance half width and quality factor to account for changes in the speed of sound due to the higher Ar concentration; see Gillis et al. (2010) [35].

2.4. Particle imaging

For TEM imaging, particles were collected on lacey carbon grids using an electrostatic precipitator at 0.5 L min^{-1} flow and 8 kV collection voltage. TEM images were collected at an accelerating voltage of 20 keV.

3. Results and discussion

This investigation focuses on the measurement of highly-absorbing carbonaceous aerosol absorption spectra with known electrical mobility diameter (D_m), mass (m_p), and monomer diameters (D_{mon}, where appropriate). Water was removed prior to analysis and no coatings were added to the particles after they were formed [17]. The materials were generated from a variety of sources to quantitatively measure the variability in *MAC* spectra, as shown in Fig. 3. Nine forms of highly-absorbing carbonaceous aerosol were measured: two carbon allotropes (C_{60} and crumpled graphene

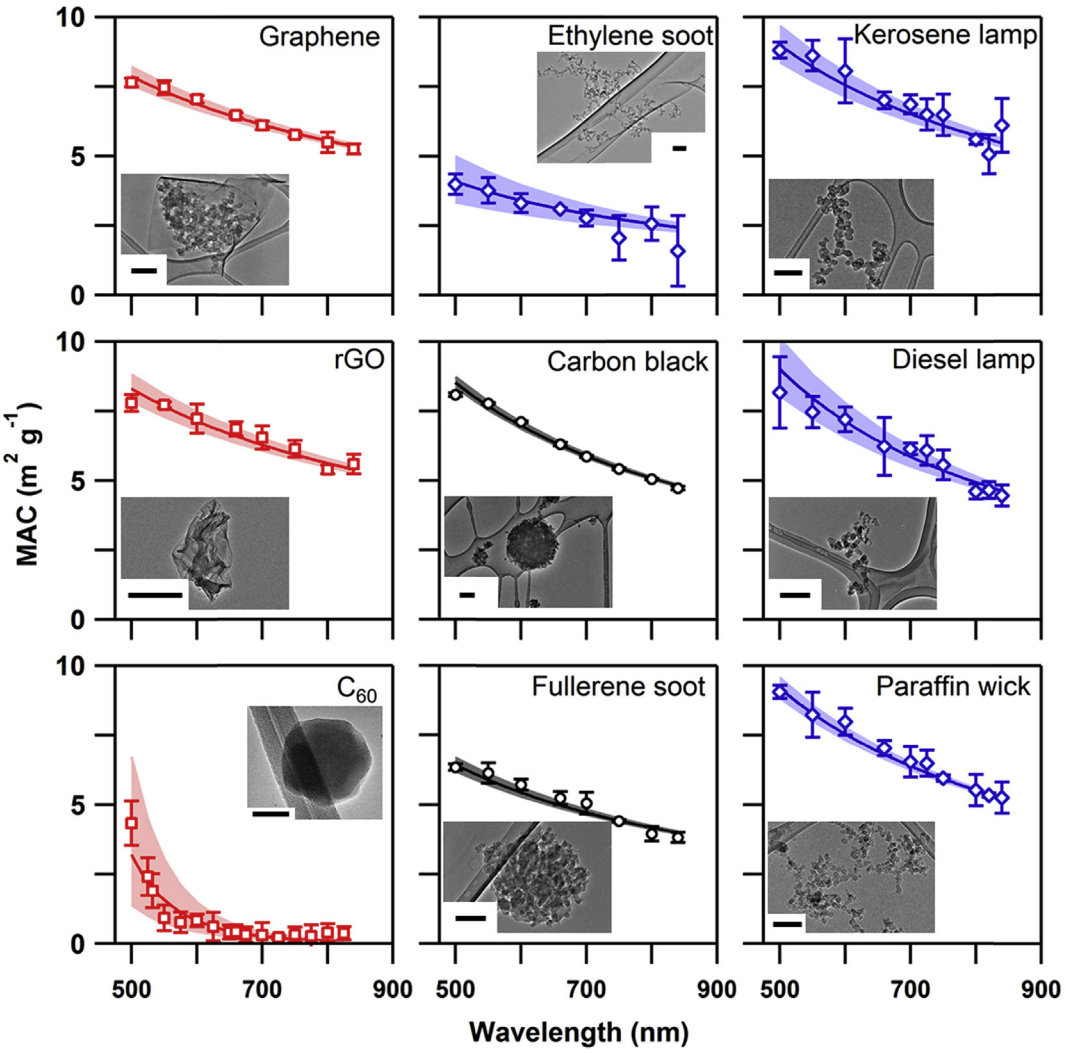

Fig. 3. Plot of mass absorption coefficients (*MAC*) for the measured particles; corresponding mobility diameters (D_m) and mass (m_p) are shown in Table 1. All plots have the same abscissa and ordinate axis ranges. Uncertainties are 2 times the standard deviation of a minimum of 3 replicate measurements. Red squares are carbon allotropes, black circles are commercially available materials, and blue diamonds are from laboratory generated particles from flames. Solid line is *AAE* determined from Eq. (2). Shaded areas represent fit uncertainties in $MAC_{\lambda,0}$ and *AAE*, see Table 1. Insets in each plot show the corresponding TEM images. Scale bars are 200 nm. (For interpretation of the references to colour in this figure legend, the reader is referred to the web version of this article.)

sheets) and seven types of amorphous carbon consisting of spark-discharge fullerene soot [36], thermally reduced graphene oxide (rGO), carbon black, and particles generated from gas (ethylene), liquid (kerosene and diesel) and solid (paraffin) fuel sources. Absorption spectra for each material were measured at the maximum α_{abs} (maximum $\alpha_{abs} = NC_{abs}$ for each sample) where the desired $q = +1$ particles could be isolated from the polydisperse distribution [33]. Note that the spectral response of some of the measured materials may be dependent on particle size (electrical mobility), monomer size and/or sheet lateral dimensions, see discussion below. Particles from each sample were collected on lacey carbon grids for TEM imaging; see Fig. 3 insets. Additional TEM images are included in the Supplementary Data. Particles from ethylene, kerosene, diesel and paraffin fueled flames possessed lacey aggregate morphologies with low effective densities ($\rho_{eff} < 0.2\ g\ cm^{-3}$). The size and distribution of D_{mon} was determined from TEM images of each material and was fuel type dependent, see Table 1. Water-soluble carbon black particles were generated from combustion of carbonaceous fuels followed by rapid surface oxidization. The resulting particles consisted of well-defined aggregated monomers arranged into a nearly-spherical morphology with $\rho_{eff} = 0.77\ g\ cm^{-3}$, similar in structure to compacted or aged flame-generated particles observed in the atmosphere and laboratory [3–5,37,38]. Fullerene soot was formed from the spark discharge of elemental carbon in the absence of O_2 forming particles with comparable morphology and effective density to carbon black [39], but with oblong, necked, and poorly-defined monomers preventing the determination of D_{mon}. Similar to previous studies [6–9], rGO was composed of multilayered graphene-like sheets with a crumpled nanopaper morphology. Graphene aerosol possessed a similar morphology to rGO with the addition of some soot-like aggregated monomers produced during the formation process. C_{60} aerosol was arranged into close packed spheres (packing density = 0.73) [26].

Mass absorption coefficient spectra were measured between $\lambda = 500$ nm and 840 nm (see Fig. 3) using a photoacoustic spectrometer and a broadband supercontinuum laser source [16]. Particles atomized from aqueous solution had a factor of ≈5 lower uncertainty than particles generated from flames. All spectra possessed a minimum of 8 data points allowing for *AAE* to be fit using Eq. (2). The *MAC* at $\lambda = 550$ nm ranged between $0.9\ m^2\ g^{-1}$

Table 1
Measured mobility diameter (D_m), mass (m_p), effective density (ρ_{eff}), mean monomer diameter (D_{mon}), measured *MAC* ($\lambda = 550$ nm), fit $MAC_{\lambda,0}$ ($\lambda_0 = 840$ nm, see Eq. (2)) and *AAE* for all particle types. Uncertainties shown in parenthesis are 2σ.

Species	D_m (nm)	m_p ($x10^{-15}$ g)	ρ_{eff} (g cm^{-3})	D_{mon} (nm)	$MAC_{Measured}$ ($\lambda = 550$ nm)	$MAC_{\lambda,0}$ ($\lambda = 840$ nm)	*AAE*
Ethylene soot	250	1.47	0.18	17 (3)	3.8 (0.5)	2.4 (0.2)	1.0 (0.3)
Kerosene lamp	700	21.0	0.12	42 (12)	8.6 (0.6)	5.5 (0.2)	1.0 (0.1)
Diesel lamp	700	21.0	0.12	26 (8)	7.5 (0.6)	4.6 (0.2)	1.3 (0.2)
Paraffin wick	700	23.6	0.13	28 (11)	8.2 (0.8)	5.2 (0.1)	1.1 (0.1)
Carbon black[a]	250	6.15	0.77	27 (7)	7.78 (0.06)	4.80 (0.04)	1.11 (0.03)
Graphene	450	23.5	0.51	–	7.5 (0.1)	5.35 (0.08)	0.74 (0.05)
Reduced GO	250	6.40	0.82	–	7.7 (0.1)	5.4 (0.1)	0.83 (0.07)
Fullerene soot	350	16.6	0.74	–	6.1 (0.4)	3.99 (0.06)	0.92 (0.05)
C_{60}	150	2.20	1.2	–	0.9 (0.5)	0.07 (0.02)	7.5 (0.9)

[a] H_2O soluble material. Does not meet operational definition of BC given in Ref. [18].

and 8.6 m^2 g^{-1} (see Table 1). The measured *MAC* of carbon black, rGO and graphene were within 2σ of particles generated from lamp and wick sources at $\lambda = 550$ nm, however their measured *AAE*'s were not. C_{60} had a *MAC* and *AAE* of 0.9 ± 0.5 m^2 g^{-1} and 7.5 ± 0.9, respectively, that exhibited a statistically significant difference from all other materials.

The *MAC* of flame-generated particles (ethylene, kerosene, diesel, and paraffin) ranged between 3.8 m^2 g^{-1} and 8.6 m^2 g^{-1}; the *MAC* of particles generated from ethylene were statistically different than the measured *MAC* of other flame-generated particles. The *AAE* of particles generated from diesel fueled simple wick lamps were also statistically different from the other flame-generated particles ($p < 0.05$).

It has been noted that the *MAC* of particles produced from high-temperature flames, such as ethylene, are highly variable due to the quenching of particle oxidation by a rapidly flowing, cool gas at the flame terminus [3,16,40]. Small changes in particle formation conditions can greatly impact particle concentrations and spectral properties [3]. The *MAC* for ethylene presented in this study are comparable to previous reports in this laboratory using fuel flow conditions where particle concentration and α_{abs} were maximized and intra- and inter-day variability and uncertainty in *MAC* were minimized [3,37].

The parameters that influence the spectroscopy of graphene-like materials in spherical structures with a high imaginary component of the refractive index (k) has been previously described in detail by Moosmüller et al. [10,11]. It is important to note that the measured absorption per unit mass of highly-absorbing carbonaceous aerosol is a function the primary, secondary and tertiary structures of the material [41–44]; see Fig. 4a. The intrinsic absorption strength of a material is a function of its chemical composition (i.e. refractive index); for graphitic and graphenic materials, this refers to the extent of sp^2-bonding, surface imperfections and single sheet lateral dimension. Absorption by the primary structures can be enhanced or dampened depending upon their atomistic arrangement into secondary structure(s) as spheres, multilayered sheets, etc. The collection of secondary structures into a final tertiary morphology can further impact absorption strength. Fig. 4b shows Mie theory calculations that simulate the effect of material primary structure (chemistry) on absorption strength per unit mass (*MAC*) by changing the imaginary component of the refractive index (k) with a constant real component ($n = 1.77$); monomer diameter ($D_{mon} = 1$ nm) and mass density ($\rho = 1.65$ g cm^{-3}); this D_{mon} and ρ approximates a single C_{60} molecule. In this case, *MAC* increases monotonically with k and the spectral shape is invariant, $AAE = 1.0$, for all values of k.

The effect of secondary structure on *MAC* was also simulated for a spherical particle by changing monomer diameter (D_{mon}) at a constant refractive index ($m = 1.77 + 0.8i$) and mass density ($\rho = 1.65$ g cm^{-3}); see Fig. 4c. At $\lambda = 400$ nm the *MAC* increases by 1% between a D_{mon} of 1 nm and 10 nm and 13% between 10 nm and 50 nm. For this refractive index, monomers $\geq$10 nm in diameter are outside of the volume absorption regime (constant *MAC*). The results also show *AAE* increasing from 1.0 to 1.2 for D_{mon} between 1 nm and 100 nm. For $D_{mon} \geq 100$ nm, the spectral dependence may not be adequately captured by an *AAE* (Eq. (2)).

The effect of tertiary structure (i.e. morphology) on *MAC* for a collection of monomers is also significant. However, calculating *MAC* with elaborate particle geometries is a computational challenge best addressed using complex optical routines such as the discrete dipoles approximation and the superposition T-matrix method as described in studies by Mishchenko and Mackowski, among others [45–49].

These Mie theory calculations assume the simplest case using monodisperse spherical monomers, but help to capture the complexity and challenge of quantitative measurement, reporting, and comparison of highly-absorbing carbonaceous aerosol spectral data. In this investigation, the D_{mon} of flame-generated particles ranged between 17 nm (ethylene soot) and 42 nm (kerosene lamp). Mie theory calculations over this range show that the *MAC* and *AAE* increase nearly linearly with D_{mon} at constant refractive index (see Supplemental Data Fig. S3), with the *MAC* and *AAE* of 42 nm diameter monomers nearly 6% and 12% higher than 17 nm monomers, respectively. Thus, the difference in *MAC* and *AAE* between particles generated from ethylene fueled flames and wick lamps, with the only difference being the fuel used, cannot be explained solely by D_{mon}. As all flame-generated particles had comparable morphology, the measured differences in *MAC* and *AAE* are likely due to differences in the refractive indices of each material under the measured formative conditions.

The definition of BC has 4 measurable properties [18]: 1) composed of aggregates of small carbon spherules, 2) $MAC \geq 5$ m^2 g^{-1} at $\lambda = 550$ nm, 3) refractory with a vaporization temperature near 4000 K, 4) insoluble in water and common organic solvents. Properties 1 and 2 were directly measured in this investigation. Despite some materials having formative conditions consistent with BC, only three of the nine samples met both the morphological and spectroscopic definitions of BC (particles generated from kerosene and diesel lamps, and the paraffin wax candle), see text in Table 1. The particles produced in this investigation from an ethylene fueled flame did not meet the spectroscopic definition for BC, whereas graphene and rGO did not meet the morphological definition. Carbon black met the morphological and spectroscopic definitions but its water solubility negates its inclusion.

As shown in Fig. 4a, in addition to being dependent on material refractive index and D_{mon}, *MAC* is also a function of morphology and/or D_m. It can be envisioned that particles with a lacey morphology – e.g. freshly-emitted flame-generated particles – with small D_{mon} enables light to access the entire particle resulting

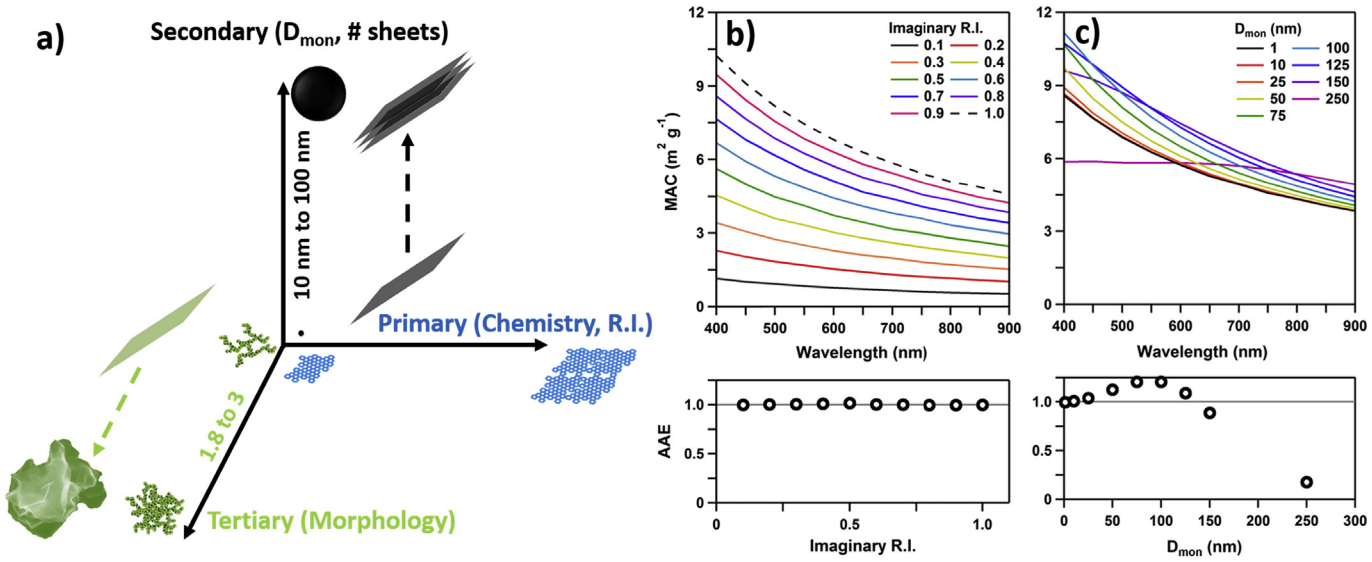

Fig. 4. a) Mass absorption coefficients (*MAC*) of carbonaceous particles are a function of primary (refractive index), secondary (atomistic arrangement), and tertiary structures (particle morphology). b) *MAC* and absorption Ångström exponent (*AAE*) as a function of imaginary component of the refractive index for particles with a real component of the refractive index = 1.77, 1 nm monomer diameter (D_{mon}) and 1.65 g cm^{-1} mass density. c) *MAC* and *AAE* as a function of D_{mon} at constant refractive index ($m = 1.77 + 0.8i$).

in absorption that scales linearly with particle mass (volume) for all D_m. In contrast, particles with a compacted morphology may only be in the volume absorption regime (constant *MAC* and *AAE)* at very small mobility diameters (D_m) and transition to the Mie or geometric absorption regimes with increasing D_m, resulting in both parameters being a function of D_m. Fig. 5 tests this hypothesis by measuring the change (Δ) in *MAC* and *AAE* as a function of D_m between $\lambda = 532$ nm and 780 nm for mass- and mobility-selected particles (21 samples) of multilayered crumpled sheets (rGO), compacted flame-generated particles (carbon black) and freshly formed, lacey particles generated from an ethylene flame with $D_{mon} \approx 20$ nm. Particles generated from the ethylene flame were measured between 300 nm $\leq D_m \leq$ 550 nm where it was assured only singly-charged particles were isolated from the distribution [3,33]. The *MAC* of the crumpled sheets and compacted spherical particles decreases nearly monotonically with D_m, consistent with geometric absorption even for the smallest particles measured ($D_m = 150$ nm). A similar dependence was measured for the change in *AAE* with D_m for crumpled and compacted particles, see Fig. 4b. For particles generated from an ethylene flame, the *MAC* and *AAE* are constant within measurement uncertainty for particles up to $D_m = 550$ nm and typical of particles in the volumetric absorption regime. These data confirm that particle morphology impacts the spectral properties of highly-absorbing carbonaceous particles. For flame-generated particles where D_{mon} is small and the morphology is consistent with an open, lacey structure (fractal dimension, $D_f \approx 1.8$ [50]) it is reasonable to assume that the particle absorption scales directly with particle mass and *MAC* and *AAE* are invariant. For particles that fall outside of this narrow parameter space this assumption may not be valid.

Many studies have focused on the measurement and reporting of *MAC* for highly-absorbing carbonaceous (BC-like) particles in the atmosphere since the first assessment of BC *MAC* [1]. Fig. 6 shows the absorption spectra collected in this investigation, with the exception of C_{60}, and all the peer-reviewed *MAC* data (1971–2018, 199 measured values) for materials reported as BC or soot, including 26 measurements of graphite and graphene allotropes of

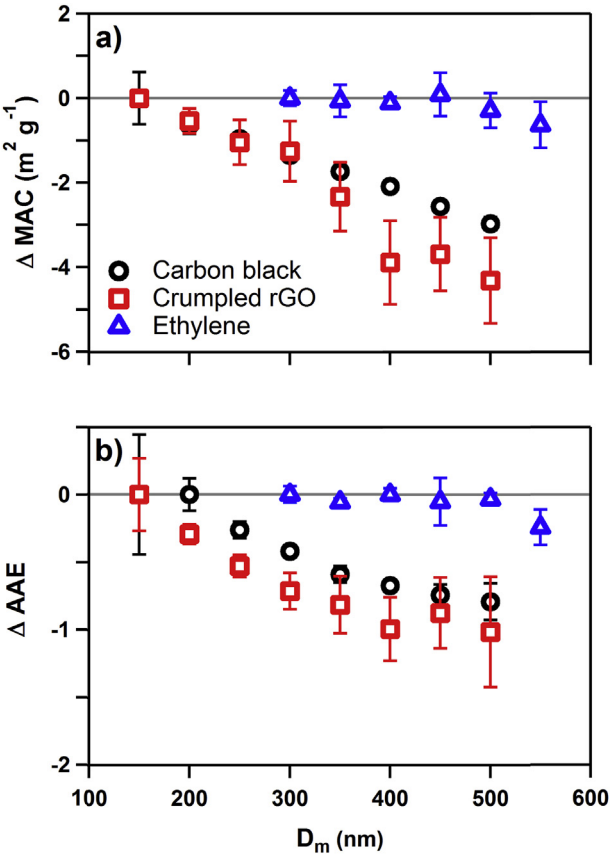

Fig. 5. a) Change (Δ) in the mass absorption coefficient (*MAC*) at $\lambda = 532$ nm and b) change (Δ) in absorption Ångström exponent (*AAE*) between $\lambda = 532$ nm and 780 nm as function of particle mobility diameter (D_m) for compact carbon black (red squares), crumpled rGO (black circles), and fresh, lacey particles from ethylene flame (blue circles). Error bars are 1 standard deviation of a minimum of 3 replicate measurements. (For interpretation of the references to colour in this figure legend, the reader is referred to the web version of this article.)

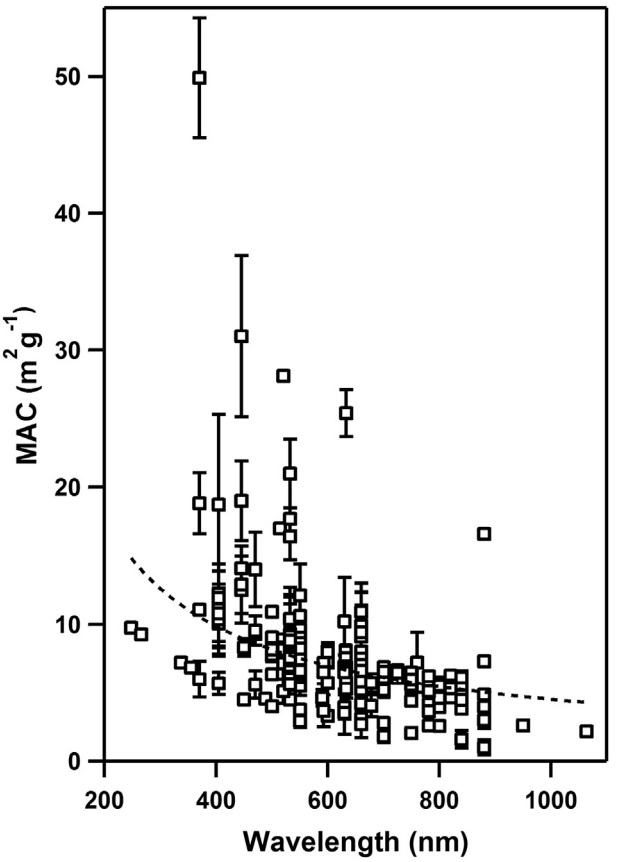

Fig. 6. All published *MAC* data of BC, soot and allotropes of carbon between 1971 to current as a function of wavelength. Error bars are 1σ. Dashed line is fit to Eq. (2) – Data from Refs. [3,12,36,38,51–77].

carbon [3,12,36,38,51–77]. The reported data include both laboratory measurements of characterized systems from known sources such as coal combustion, kerosene wick lamps, diesel engines, diffusion flames, and spark discharge soot with known carbon-to-oxygen ratios and data from field-based observations from sites such as traffic tunnels and urban areas. The data are shown at the wavelength reported in each study with 1σ uncertainty (if reported). The published data include 129 *MAC* values measured using photoacoustic spectroscopy (PAS), 36 reports from filter-based methods, and 29 reports which used extinction minus scattering. The range of data extends from 248 nm $\leq \lambda \leq$ 1064 nm, enabling the use of Eq. (2) to determine *AAE* and *MAC*.

The *MAC* of the previously published data is highly variable. For example, at $\lambda = 532$ nm (24 samples) the *MAC* of all published data ranges between $5.61 \pm 0.46\ m^2\ g^{-1}$ and $21.0 \pm 2.5\ m^2\ g^{-1}$, (average $= 8.31 \pm 0.89\ m^2\ g^{-1}$) larger than the variability in *MAC* for the carbonaceous materials measured in this study. The published data was also examined by the source of the material. Aerosol generated from diesel engines represents the largest single source of reported *MAC* data (19 reported *MAC* values). The reported range in *MAC* from diesel engine generated aerosol for 514 nm $\leq \lambda \leq$ 532 nm (7 samples) is $7.4 \pm 0.5\ m^2\ g^{-1}$ to $17\ m^2\ g^{-1}$ (no reported uncertainty) with an average of $9.5 \pm 3.3\ m^2\ g^{-1}$.

The *AAE* of the all data shown in Fig. 6 was calculated using Eq. (2) as 1.01 ± 0.15 (1σ), within uncertainty of 1.0 suggested in Bond and Bergstrom (2006) and in support of the λ^{-1} dependence [1,3,10,11,18]. The *MAC* of the population using all the published data at $\lambda = 550$ nm is $8.28 \pm 0.34\ m^2\ g^{-1}$, 10% higher than the previous assessment of BC *MAC*, with uncertainty reduced by a factor of 4, see Table 2.

Some of the published *MAC* data was more than 5σ from the mean, greatly increasing the uncertainty in both *AAE* and *MAC*, and are likely not physical (e.g. $MAC = 50\ m^2\ g^{-1}$ at $\lambda = 370$ nm) based on *MAC* calculated from refractive indices and D_{mon} using Mie theory. The published data shows a dependence on the method utilized for analysis, see Table 2. For example, using only PAS data yields $MAC = 8.03 \pm 0.31\ m^2\ g^{-1}$ and $AAE = 0.84 \pm 0.13$, whereas using data from filter-based studies results in $MAC = 9.67 \pm 1.50\ m^2\ g^{-1}$ and $AAE = 1.83 \pm 0.56$. Curation of all the data via elimination of data outside of the average *MAC* + 5σ (9 points removed) results in a 50% reduction in the reported uncertainty for the *MAC*, with $MAC = 7.52 \pm 0.18\ m^2\ g^{-1}$ and $AAE = 0.85 \pm 0.09$, within 1σ of *MAC* but with a lower *AAE* than reported in the BC assessments [1,18].

4. Conclusions

The presented data highlight *MAC* variability of highly-absorbing carbonaceous aerosol. BC has been previously defined as a material with a well-defined refractive index and *MAC* that can be assigned defined values (e.g. BC refractive index = 1.95 + 0.79*i*, $MAC = 7.5 \pm 1.2\ m^2\ g^{-1}$) [1], similar to other well-defined nanomaterials such as SiO_2 or polystyrene spheres that have been used for standards. If a single *MAC* value exists for BC and other similar materials, it would be expected that its reported range would be narrow; see data at $\lambda = 532$ nm and 660 nm in Fig. 6 where adequate data exists for comparison between studies. The range in published *MAC* observations suggests that either: 1) the reported data is dominated by measurement errors and biases and that the *MAC* of BC and other similar materials is well-defined and invariant across formative conditions or 2) the reported data captures the spectral variability and that highly-absorbing carbonaceous aerosol exists within a range of chemical and physical properties that impact particle absorption. Based on the measurements presented in this study for particles with known D_m, D_{mon}, m_p, and morphology it is likely the observed spectral variability in highly-absorbing carbonaceous aerosol is due to the impact of material refractive index, D_{mon}, and, in some cases, particle morphology that

Table 2
Fit parameters calculated from Eq. (2) of published carbonaceous aerosol *MAC* between 1971 and 2018. Fit parameters also reported for published PAS and filter-based measurements and after removal of outlier data > 5σ from mean. Uncertainties are 1σ and shown in parenthesis.

	k_0 ($\lambda = 550$ nm, $m^2\ g^{-1}$)	*AAE*
All published measurements	8.28 (0.34)	1.01 (0.15)
All published PAS	8.03 (0.31)	0.84 (0.13)
All published Filter-based	9.67 (1.50)	1.83 (0.56)
All measurements − 5σ outliers removed	7.52 (0.18)	0.85 (0.09)
PAS − 5σ outliers removed	7.39 (0.19)	0.76 (0.19)
Filter-based − 5σ outliers removed	7.40 (0.53)	1.31 (0.28)

result from the diversity of formative conditions for this family of materials.

Acknowledgements

The authors thank Yong Yang at the University of Maryland for assistance in acquisition of TEM images of some of samples.

Appendix A. Supplementary data

Supplementary Data includes Mie theory calculations of *MAC* and as a function of D_{mon}, and TEM images of particles.

Supplementary data related to this article can be found at https://doi.org/10.1016/j.carbon.2018.04.057.

References

[1] T.C. Bond, R.W. Bergstrom, Light absorption by carbonaceous particles: an investigative review, Aerosol. Sci. Technol. 40 (1) (2006) 27–67.
[2] P.R. Buseck, K. Adachi, A. Gelencsér, É. Tompa, M. Pósfai, Ns-soot: a material-based term for strongly light-absorbing carbonaceous particles, Aerosol. Sci. Technol. 48 (7) (2014) 777–788.
[3] J.G. Radney, R. You, X. Ma, J.M. Conny, M.R. Zachariah, J.T. Hodges, et al., Dependence of soot optical properties on particle morphology: measurements and model comparisons, Environ. Sci. Technol. 48 (6) (2014) 3169–3176.
[4] X. Ma, C.D. Zangmeister, J. Gigault, G.W. Mulholland, M.R. Zachariah, Soot aggregate restructuring during water processing, J. Aerosol Sci. 66 (2013) 209–219.
[5] J. Peng, M. Hu, S. Guo, Z. Du, J. Zheng, D. Shang, et al., Markedly enhanced absorption and direct radiative forcing of black carbon under polluted urban environments, Proc. Natl. Acad. Sci. U. S. A. 113 (16) (2016) 4266–4271.
[6] X. Ma, M.R. Zachariah, C.D. Zangmeister, Crumpled nanopaper from graphene oxide, Nano Lett. 12 (1) (2011) 486–489.
[7] X. Ma, M.R. Zachariah, C.D. Zangmeister, Reduction of suspended graphene oxide single sheet nanopaper: the effect of crumpling, J. Phys. Chem. C 117 (6) (2013) 3185–3191.
[8] W.-N. Wang, Y. Jiang, P. Biswas, Evaporation-induced crumpling of graphene oxide nanosheets in aerosolized droplets: confinement force relationship, J. Phys. Chem. Lett. 3 (21) (2012) 3228–3233.
[9] H. Yang, Y. Wang, Y. Song, L. Qiu, S. Zhang, D. Li, et al., Assembling of graphene oxide in an isolated dissolving droplet, Soft Matter 8 (44) (2012) 11249–11254.
[10] H. Moosmüller, W.P. Arnott, Particle optics in the Rayleigh regime, J. Air Waste Manage. Assoc. 59 (9) (2009) 1028–1031.
[11] H. Moosmüller, R.K. Chakrabarty, W.P. Arnott, Aerosol light absorption and its measurement: a review, J. Quant. Spectrosc. Radiat. Transfer 110 (11) (2009) 844–878.
[12] H. Moosmüller, W.P. Arnott, C.F. Rogers, J.C. Chow, C.A. Frazier, L.E. Sherman, et al., Photoacoustic and filter measurements related to aerosol light absorption during the northern front range air quality study (Colorado 1996/1997), J. Geophys. Res. Atmos. 103 (D21) (1998) 28149–28157.
[13] B. Srinivas, N. Rastogi, M.M. Sarin, A. Singh, D. Singh, Mass absorption efficiency of light absorbing organic aerosols from source region of paddy-residue burning emissions in the indo-gangetic plain, Atmos. Environ. 125 (Part B) (2016) 360–370.
[14] R.K. Chakrabarty, M. Gyawali, R.L.N. Yatavelli, A. Pandey, A.C. Watts, J. Knue, et al., Brown carbon aerosols from burning of boreal peatlands: microphysical properties, emission factors, and implications for direct radiative forcing, Atmos. Chem. Phys. 16 (5) (2016) 3033–3040.
[15] L. Caponi, P. Formenti, D. Massabó, C. Di Biagio, M. Cazaunau, E. Pangui, et al., Spectral- and size-resolved mass absorption efficiency of mineral dust aerosols in the shortwave spectrum: a simulation chamber study, Atmos. Chem. Phys. 17 (11) (2017) 7175–7191.
[16] J.G. Radney, C.D. Zangmeister, Measurement of gas and aerosol phase absorption spectra across the visible and near-ir using supercontinuum photoacoustic spectroscopy, Anal. Chem. 87 (14) (2015) 7356–7363.
[17] R. You, J.G. Radney, M.R. Zachariah, C.D. Zangmeister, Measured wavelength-dependent absorption enhancement of internally mixed black carbon with absorbing and nonabsorbing materials, Environ. Sci. Technol. 50 (15) (2016) 7982–7990.
[18] T.C. Bond, S.J. Doherty, D.W. Fahey, P.M. Forster, T. Berntsen, B.J. DeAngelo, et al., Bounding the role of black carbon in the climate system: a scientific assessment, J. Geophys. Res. Atmos. 118 (2013) 5380–5552.
[19] V. Ramanathan, G. Carmichael, Global and regional climate changes due to black carbon, Nat. Geosci. 1 (4) (2008) 221–227.
[20] T. Ajtai, N. Utry, M. Pintér, B. Major, Z. Bozóki, G. Szabó, A method for segregating the optical absorption properties and the mass concentration of winter time urban aerosol, Atmos. Environ. 122 (2015) 313–320.
[21] N. Utry, T. Ajtai, Á. Filep, M. Pintér, Z. Török, Z. Bozóki, et al., Correlations between absorption angström exponent (aae) of wintertime ambient urban aerosol and its physical and chemical properties, Atmos. Environ. 91 (2014) 52–59.
[22] D. Baumgardner, O. Popovicheva, J. Allan, V. Bernardoni, J. Cao, F. Cavalli, et al., Soot reference materials for instrument calibration and intercomparisons: a workshop summary with recommendations, Atmos. Meas. Tech. 5 (8) (2012) 1869–1887.
[23] J.G. Slowik, E.S. Cross, J.-H. Han, P. Davidovits, T.B. Onasch, J.T. Jayne, et al., An inter-comparison of instruments measuring black carbon content of soot particles, Aerosol. Sci. Technol. 41 (3) (2007) 295–314.
[24] NIST technical disclaimer: Certain commercial equipment, instruments, or materials (or suppliers, or software,...) are identified in this paper to foster understanding. Such identification does not imply recommendation or endorsement by the National Institute of Standards and Technology, nor does it imply that the materials or equipment identified are necessarily the best available for the purpose.
[25] C.D. Zangmeister, Preparation and evaluation of graphite oxide reduced at 220 °C, Chem. Mater. 22 (19) (2010) 5625–5629.
[26] A.S. Gurav, T.T. Kodas, L.-M. Wang, E.I. Kauppinen, J. Joutsensaari, Generation of nanometer-size fullerene particles via vapor condensation, Chem. Phys. Lett. 218 (4) (1994) 304–308.
[27] R.J. Santoro, H.G. Semerjian, R.A. Dobbins, Soot particle measurements in diffusion flames, Combust. Flame 51 (0) (1983) 203–218.
[28] J. Apple, R. Vicente, A. Yarberry, N. Lohse, E. Mills, A. Jacobson, et al., Characterization of particulate matter size distributions and indoor concentrations from kerosene and diesel lamps, Indoor Air 20 (5) (2010) 399–411.
[29] N.L. Lam, Y. Chen, C. Weyant, C. Venkataraman, P. Sadavarte, M.A. Johnson, et al., Household light makes global heat: high black carbon emissions from kerosene wick lamps, Environ. Sci. Technol. 46 (24) (2012) 13531–13538.
[30] J.G. Radney, C.D. Zangmeister, Light source effects on aerosol photoacoustic spectroscopy measurements, J. Quant. Spectrosc. Radiat. Trans. 187 (2017) 145–149.
[31] J.M. Langridge, M.S. Richardson, D.A. Lack, C.A. Brock, D.M. Murphy, Limitations of the photoacoustic technique for aerosol absorption measurement at high relative humidity, Aerosol. Sci. Technol. 47 (11) (2013) 1163–1173.
[32] J.G. Radney, X. Ma, K.A. Gillis, M.R. Zachariah, J.T. Hodges, C.D. Zangmeister, Direct measurements of mass-specific optical cross sections of single component aerosol mixtures, Anal. Chem. 85 (17) (2013) 8319–8325.
[33] J.G. Radney, C.D. Zangmeister, Practical limitations of aerosol separation by a tandem differential mobility analyzer–aerosol particle mass analyzer, Aerosol. Sci. Technol. 50 (2) (2016) 160–172.
[34] J.G. Radney, R. You, M.R. Zachariah, C.D. Zangmeister, Direct in situ mass specific absorption spectra of biomass burning particles generated from smoldering hard and softwoods, Environ. Sci. Technol. 51 (10) (2017) 5622–5629.
[35] K.A. Gillis, D.K. Havey, J.T. Hodges, Standard photoacoustic spectrometer: model and validation using o2 a-band spectra, Rev. Sci. Instrum. 81 (6) (2010) 064902–064913.
[36] M. Schnaiter, H. Horvath, O. Möhler, K.H. Naumann, H. Saathoff, O.W. Schöck, Uv-vis-nir spectral optical properties of soot and soot-containing aerosols, J. Aerosol Sci. 34 (10) (2003) 1421–1444.
[37] P.A. Bueno, D.K. Havey, G.W. Mulholland, J.T. Hodges, K.A. Gillis, R.R. Dickerson, et al., Photoacoustic measurements of amplification of the absorption cross section for coated soot aerosols, Aerosol. Sci. Technol. 45 (10) (2011) 1217–1230.
[38] R. Zhang, A.F. Khalizov, J. Pagels, D. Zhang, H. Xue, P.H. McMurry, Variability in morphology, hygroscopicity, and optical properties of soot aerosols during atmospheric processing, Proc. Natl. Acad. Sci. U. S. A. 105 (30) (2008) 10291–10296.
[39] N. Moteki, Y. Kondo, N. Takegawa, S.-I. Nakamura, Directional dependence of thermal emission from nonspherical carbon particles, J. Aerosol Sci. 40 (9) (2009) 790–801.
[40] R.H. Moore, L.D. Ziemba, D. Dutcher, A.J. Beyersdorf, K. Chan, S. Crumeyrolle, et al., Mapping the operation of the miniature combustion aerosol standard (mini-cast) soot generator, Aerosol. Sci. Technol. 48 (5) (2014) 467–479.
[41] C. García Fernández, S. Picaud, M. Devel, Calculations of the mass absorption cross sections for carbonaceous nanoparticles modeling soot, J. Quant. Spectrosc. Radiat. Trans. 164 (Supplement C) (2015) 69–81.
[42] R. Langlet, M.R. Vanacharla, S. Picaud, M. Devel, Bottom-up multi-step approach to study the relations between the structure and the optical properties of carbon soot nanoparticles, J. Quant. Spectrosc. Radiat. Trans. 110 (14) (2009) 1615–1627.
[43] F. Moulin, M. Devel, S. Picaud, Optical properties of soot nanoparticles, J. Quant. Spectrosc. Radiat. Transfer 109 (10) (2008) 1791–1801.
[44] B.V. Scarnato, S. Vahidinia, D.T. Richard, T.W. Kirchstetter, Effects of internal mixing and aggregate morphology on optical properties of black carbon using a discrete dipole approximation model, Atmos. Chem. Phys. 13 (10) (2013) 5089–5101.
[45] W.R. Heinson, A. Chakrabarti, C.M. Sorensen, Divine proportion shape invariance of diffusion limited cluster–cluster aggregates, Aerosol. Sci. Technol. 49 (9) (2015) 786–792.
[46] Y.W. Heinson, J.B. Maughan, W.R. Heinson, A. Chakrabarti, C.M. Sorensen, Light scattering q-space analysis of irregularly shaped particles, J. Geophys. Res. Atmos. 121 (2) (2016) 682–691.
[47] M.I. Mishchenko, D.W. Mackowski, L.D. Travis, Scattering of light by bispheres with touching and separatedcomponents, Appl. Opt. 34 (21) (1995)

4589–4599.
[48] K. Skorupski, The optical properties of tropospheric soot aggregates determined with the DDA (discrete dipole approximation) method, SPIE Optical Metrology SPIE (2015) 10.
[49] C. Sorensen, Y. Heinson, W. Heinson, J. Maughan, A. Chakrabarti, Q-space analysis of the light scattering phase function of particles with any shape, Atmosphere 8 (4) (2017) 68.
[50] C.M. Sorensen, Light scattering by fractal aggregates: a review, Aerosol. Sci. Technol. 35 (2) (2001) 648–687.
[51] C.W. Bruce, T.F. Stromberg, K.P. Gurton, J.B. Mozer, Trans-spectral absorption and scattering of electromagnetic radiation by diesel soot, Appl. Opt. 30 (12) (1991) 1537–1546.
[52] C.E. Chung, S.W. Kim, M. Lee, S.C. Yoon, S. Lee, Carbonaceous aerosol aae inferred from in-situ aerosol measurements at the gosan abc super site, and the implications for brown carbon aerosol, Atmos. Chem. Phys. 12 (14) (2012) 6173–6184.
[53] I. Colbeck, B. Atkinson, Y. Johar, The morphology and optical properties of soot produced by different fuels, J. Aerosol Sci. 28 (5) (1997) 715–723.
[54] I. Colbeck, E.J. Hardman, R.M. Harrison, Optical and dynamical properties of fractal clusters of carbonaceous smoke, J. Aerosol Sci. 20 (7) (1989) 765–774.
[55] E.S. Cross, T.B. Onasch, A. Ahern, W. Wrobel, J.G. Slowik, J. Olfert, et al., Soot particle studies - instrument inter-comparison - project overview, Aerosol. Sci. Technol. 44 (8) (2010) 592–611.
[56] X. Cui, X. Wang, L. Yang, B. Chen, J. Chen, A. Andersson, et al., Radiative absorption enhancement from coatings on black carbon aerosols, Sci. Total Environ. 551–552 (Supplement C) (2016) 51–56.
[57] J. Genberg, H.A.C. Denier van der Gon, D. Simpson, E. Swietlicki, H. Areskoug, D. Beddows, et al., Light-absorbing carbon in europe - measurement and modelling, with a focus on residential wood combustion emissions, Atmos. Chem. Phys. 13 (17) (2013) 8719–8738.
[58] L.A. Gundel, R.L. Dod, H. Rosen, T. Novakov, The relationship between optical attenuation and black carbon concentration for ambient and source particles, Sci. Total Environ. 36 (Supplement C) (1984) 197–202.
[59] A.F. Khalizov, H. Xue, L. Wang, J. Zheng, R. Zhang, Enhanced light absorption and scattering by carbon soot aerosol internally mixed with sulfuric acid, J. Phys. Chem. A 113 (6) (2009) 1066–1074.
[60] A. Knox, G.J. Evans, J.R. Brook, X. Yao, C.H. Jeong, K.J. Godri, et al., Mass absorption cross-section of ambient black carbon aerosol in relation to chemical age, Aerosol. Sci. Technol. 43 (6) (2009) 522–532.
[61] M. Laborde, M. Crippa, T. Tritscher, Z. Jurányi, P.F. Decarlo, B. Temime-Roussel, et al., Black carbon physical properties and mixing state in the european megacity paris, Atmos. Chem. Phys. 13 (11) (2013) 5831–5856.
[62] C. Linke, I. Ibrahim, N. Schleicher, R. Hitzenberger, M.O. Andreae, T. Leisner, et al., A novel single-cavity three-wavelength photoacoustic spectrometer for atmospheric aerosol research, Atmos. Meas. Tech. 9 (11) (2016) 5331–5346.
[63] D. Liu, M. Flynn, M. Gysel, A. Targino, I. Crawford, K. Bower, et al., Single particle characterization of black carbon aerosols at a tropospheric alpine site in Switzerland, Atmos. Chem. Phys. 10 (15) (2010) 7389–7407.
[64] G.W. Mulholland, M.Y. Choi, Measurement of the mass specific extinction coefficient for acetylene and ethene smoke using the large agglomerate optics facility, Symp. Int. Combust. Proc. 27 (1) (1998) 1515–1522.
[65] E.M. Patterson, R.M. Duckworth, C.M. Wyman, E.A. Powell, J.W. Gooch, Measurements of the optical properties of the smoke emissions from plastics, hydrocarbons, and other urban fuels for nuclear winter studies, Atmos. Environ. Part A 25 (11) (1991) 2539–2552.
[66] D.M. Roessler, F.R. Faxvog, Optoacoustic measurement of optical absorption in acetylene smoke, J. Opt. Soc. Am. 69 (12) (1979) 1699–1704.
[67] R. Röhl, W.A. McClenny, R.A. Palmer, Photoacoustic determination of optical properties of aerosol particles collected on filters: development of a method taking into account substrate reflectivity, Appl. Opt. 21 (3) (1982) 375–381.
[68] G. Saliba, R. Subramanian, R. Saleh, A.T. Ahern, E.M. Lipsky, A. Tasoglou, et al., Optical properties of black carbon in cookstove emissions coated with secondary organic aerosols: measurements and modeling, Aerosol. Sci. Technol. 50 (11) (2016) 1264–1276.
[69] M. Schnaiter, M. Gimmler, I. Llamas, C. Linke, C. Jäger, H. Mutschke, Strong spectral dependence of light absorption by organic carbon particles formed by propane combustion, Atmos. Chem. Phys. 6 (10) (2006) 2981–2990.
[70] P.J. Sheridan, W.P. Arnott, J.A. Ogren, E. Andrews, D.B. Atkinson, D.S. Covert, et al., The reno aerosol optics study: an evaluation of aerosol absorption measurement methods, Aerosol. Sci. Technol. 39 (1) (2005) 1–16.
[71] P.R. Sinha, Y. Kondo, M. Koike, J.A. Ogren, A. Jefferson, T.E. Barrett, et al., Evaluation of ground-based black carbon measurements by filter-based photometers at two arctic sites, J. Geophys. Res. Atmos. 122 (6) (2017) 3544–3572.
[72] T. Smausz, B. Kondász, T. Gera, T. Ajtai, N. Utry, M. Pintér, et al., Determination of uv–visible–nir absorption coefficient of graphite bulk using direct and indirect methods, Appl. Phys. A Mater. Sci. Process 123 (10) (2017) 633.
[73] R. Subramanian, G.L. Kok, D. Baumgardner, A. Clarke, Y. Shinozuka, T.L. Campos, et al., Black carbon over Mexico: the effect of atmospheric transport on mixing state, mass absorption cross-section, and bc/co ratios, Atmos. Chem. Phys. 10 (1) (2010) 219–237.
[74] Q.Y. Wang, R.J. Huang, J.J. Cao, X.X. Tie, H.Y. Ni, Y.Q. Zhou, et al., Black carbon aerosol in winter northeastern qinghai–Tibetan plateau, China: the source, mixing state and optical property, Atmos. Chem. Phys. 15 (22) (2015) 13059–13069.
[75] Y. Wei, L. Ma, T. Cao, Q. Zhang, J. Wu, P.R. Buseck, et al., Light scattering and extinction measurements combined with laser-induced incandescence for the real-time determination of soot mass absorption cross section, Anal. Chem. 85 (19) (2013) 9181–9188.
[76] Y. Zhou, X. Wang, X. Wu, Z. Cong, G. Wu, M. Ji, Quantifying light absorption of iron oxides and carbonaceous aerosol in seasonal snow across northern China, Atmosphere 8 (4) (2017) 63.
[77] S.D. Forestieri, T.M. Helgestad, A. Lambe, L. Renbaum-Wolff, D.A. Lack, P. Massoli, et al., Measurement and modeling of the multi-wavelength optical properties of uncoated flame-generated soot, Atmos. Chem. Phys. Discuss. 2018 (2018) 1–39.